Nuclear Engineering and Technology 54 (2022) 817–825

Contents lists available at ScienceDirect

Nuclear Engineering and Technology

journal homepage: www.elsevier.com/locate/net

Original article

Impact of molybdenum cross sections on FHR analysis

Kyle M. Ramey [a], Marat Margulis [b], Nathaniel Read [b], Eugene Shwageraus [b], Bojan Petrovic [a, *]

[a] Nuclear and Radiological Engineering, Georgia Institute of Technology, Atlanta, GA, 30332, United States
[b] Department of Engineering, University of Cambridge, Cambridge, CB2 1PZ, United Kingdom

ARTICLE INFO

Article history:
Received 18 March 2021
Received in revised form
19 August 2021
Accepted 21 September 2021
Available online 23 September 2021

Keywords:
Molten salt reactor (MSR)
Fluoride salt cooled high temperature reactor (FHR)
Molybdenum cross section
Serpent
WIMS

ABSTRACT

A recent benchmarking effort, under the auspices of the Organization for Economic Cooperation and Development (OECD) Nuclear Energy Agency (NEA), has been made to evaluate the current state of modeling and simulation tools available to model fluoride salt-cooled high temperature reactors (FHRs). The FHR benchmarking effort considered in this work consists of several cases evaluating the neutronic parameters of a 2D prismatic FHR fuel assembly model using the participants' choice of simulation tools. Benchmark participants blindly submitted results for comparison with overall good agreement, except for some which significantly differed on cases utilizing a molybdenum-bearing control rod. Participants utilizing more recently updated explicit isotopic cross sections had consistent results, whereas those using elemental molybdenum cross sections observed reactivity differences on the order of thousands of pcm relative to their peers. Through a series of supporting tests, the authors attribute the differences as being nuclear data driven from using older legacy elemental molybdenum cross sections. Quantitative analysis is conducted on the control rod to identify spectral, reaction rate, and cross section phenomena responsible for the observed differences. Results confirm the observed differences are attributable to the use of elemental cross sections which overestimate the reaction rates in strong resonance channels.

1. Introduction

Molten salt reactor (MSR) technology has received renewed design interest in the past two decades as numerous industry and research entities are actively looking to license and build MSR facilities in the coming years. A main attraction to using liquid salts as coolants is that due to their very high boiling temperature at atmospheric pressure, MSRs may benefit from having both a high thermal efficiency as well as low (near-atmospheric) operating pressure. One class of MSR designs is the fluoride salt-cooled high temperature reactor (FHR), which uses a liquid salt coolant and a solid fuel form. Drawing from their operating experience with MSRs in the late 1960s [1], Oak Ridge National Laboratory (ORNL) began development of a prismatic FHR design in the early 2000s [2] resulting in the creation of the Advanced High Temperature Reactor (AHTR) preconceptual design [3,4]. AHTR is a large-scale 3400 MW_t design with 252 hexagonal prismatic fuel assemblies. This work focuses on a pseudo-2D model of a single reflected fuel assembly, described later, while the detailed full core design is not considered.

International interest in FHR technology has created the need for modeling and simulation tools suitable for analyzing MSR systems. To assess the capabilities of existing tools, a set of benchmark studies has been developed [5] and it is referred to as "the FHR benchmark" for the remainder of the paper. Currently, seven participating institutions from four countries are contributing results: Centrum Vyzkumu Rez, Czech Republic; Georgia Institute of Technology (GT), United States; McMaster University, Canada; Pacific Northwest National Laboratory, United States; University of Cambridge (UCam), United Kingdom; University of Illinois Urbana-Champaign, United States; and Virginia Commonwealth University, United States. Comparisons of contributor submissions [6] are being performed under the auspices of the Organization for Economic Cooperation and Development (OECD) Nuclear Energy Agency (NEA), within the activities of the Working Party on Scientific Issues and Uncertainty Analysis of Reactor Systems (WPRS) and its Expert Group on Physics of Reactor Systems (EGPRS). Each institution participating in the FHR benchmark used modeling and simulation software of their choice, with both deterministic and stochastic tools represented. Nine cases representing an FHR fuel assembly

* Corresponding author. 770 State Street NW, Atlanta, GA, 30332-0405, United States.
E-mail address: bojan.petrovic@gatech.edu (B. Petrovic).

https://doi.org/10.1016/j.net.2021.09.021

under various conditions have been analyzed.

Two participating contributors to the FHR benchmark relevant for this work are GT using the stochastic 3D continuous-energy Monte Carlo transport code Serpent [7] and UCam using the deterministic Winfrith improved multigroup scheme (WIMS) code system [8]. These two participants have achieved good agreement between their results, and with the results of other participants, except for the single case involving the use of a molybdenum-bearing control rod (CR). This work focuses on and investigates the cause of these differences and provides caveats regarding molybdenum cross sections to researchers conducting work on similar MSR systems.

2. Background and initial results

FHR designs have centered primarily on two design types: pebble bed and prismatic fuel assembly. This work focuses on the latter type; specifically, an FHR design based upon the AHTR. The geometry of the FHR fuel assembly is complex to model and draws attention to need for modeling and simulations tools capable of accurately analyzing FHR systems. A goal of the FHR benchmark is to evaluate the applicability of existing methods and methodologies toward MSR designs. Initial comparisons of results from FHR benchmark participant submissions show that agreement is generally good for 2D fuel assembly studies. Cases with discrepancies are identified for further study and additional simulations beyond those used for the FHR benchmark are performed later as part of this work.

2.1. FHR fuel assembly

The hexagonal prismatic AHTR-based fuel assembly has one-third rotational symmetry, with each one-third section containing six fuel plates ("planks"). Each fuel plank has two fuel stripes containing TRISO particles, which introduces double heterogeneity into the modeling process. The complex geometry of the FHR fuel assembly along with the double heterogeneity of the TRISO fuel particles makes developing detailed models and performing simulations to obtain accurate results challenging [9–11], hence the need for a benchmarking study of an FHR design. A visualization of the FHR fuel assembly can be seen in Fig. 1.

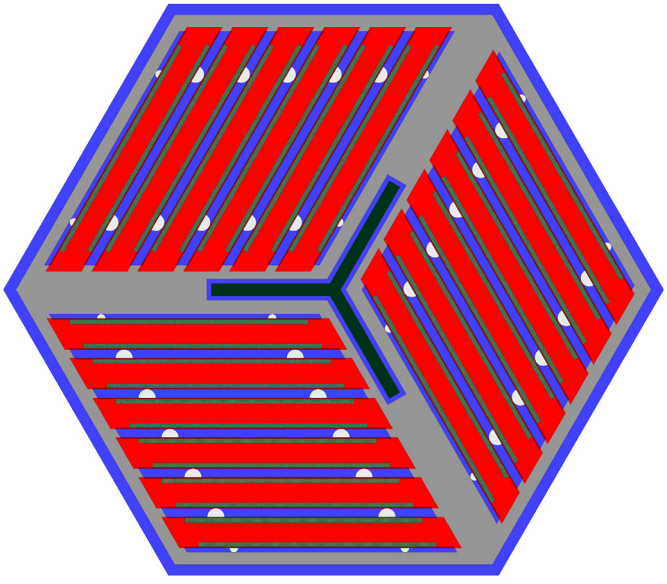

Fig. 1. FHR fuel assembly geometry.

Additional features of the FHR fuel assembly include coolant flow channels between fuel planks, semicylindrical spacers in the flow channels to separate fuel planks, columns of europia (Eu_2O_3) burnable poison for integral excess reactive control, structural carbon-carbon composite assembly wrapper and Y-shaped central structure into which the fuel planks are embedded, and a central cooling channel in the Y-shaped region. This central channel allows for the insertion of a Y-shaped CR (shown as inserted by the dark green Y-shape feature in the center of Fig. 1) made of a molybdenum-hafnium-carbon (MHC) alloy which is primarily composed of molybdenum (98.7% by weight, with 1.2% hafnium and 0.1% carbon by weight) [3]. MHC was originally proposed by ORNL and identified as the most suitable material for this type of reactor. Any significant differences observed from modeling the MHC CR are likely attributable to molybdenum cross sections.

2.2. FHR benchmark

The FHR benchmark [5] is currently being conducted under the auspices of OECD-NEA for the purpose of evaluating the accuracy and practicality of existing modeling and simulation tools for FHR systems. The benchmarking process is divided into several phases with current efforts being used to complete Phase I, which is focused on fuel assembly studies. Phase I is divided into three parts:

- Phase I-A: "2D" (pseudo-2D) fuel assembly model, steady state (no depletion)
- Phase I–B: 2D fuel assembly model depletion
- Phase 1-C: 3D fuel assembly model depletion

Due to the spherical geometry used for both fuel and burnable poison (BP) particles, a true 2D model is not feasible. Instead, pseudo-2D models use axial reflection with finite explicit particle geometry to achieve an infinite axial model for 2D studies. Phase I-A and Phase I–B have been completed by benchmark participants and work toward finishing Phase I–C is currently underway. The focus of this paper is on differences in the multiplication factor observed in the set of nine test cases used within Phase I-A of benchmark testing. The reference Case 1 assumes 9 wt% fuel enrichment, no BP, CR withdrawn, and hot full power (HFP) temperature distribution as the reference case. Variations from the reference Case 1 in other cases are noted:

- Case 1: Reference case
- Case 2H: Hot zero power (HZP) temperatures
- Case 2C: Cold zero power (CZP) temperatures
- Case 3: CR inserted
- Case 4: Discrete europia BP
- Case 4R: Discrete europia BP and CR inserted
- Case 5: Integral (dispersed) europia BP
- Case 6: Twice HM loading (fuel stripe thickness doubled)
- Case 7: Fuel enrichment increased to 19.75 wt%

For each test case, several reactor physics parameters were calculated and reported by participants. These parameters include: multiplication factor, reactivity coefficients, spatial fission distribution, flux distribution, and neutron spectrum. The sets of results from two benchmark participants will be explored further: GT using stochastic Serpent with ENDF/B-VII.0 data [12] and UCam using deterministic WIMS (version WIMS11a_dv23, but results were cross-compared and identical to WIMS10) with JEFF-3.1.2 data [13]. As a note, an ENDF/B-VII.0 based library exists for WIMS but was not used in this work, since every participant in the benchmark used their standardly used library. Future analysis may benefit from

including this analysis.

The WIMS model utilizes the multicell approach [14] which splits the FHR model into several separate cells (fuel, graphite matrix, and CR). The routine includes generation of homogenous data for each zone, followed by a merge protocol which calculates the collision probabilities between the different cells by creating a collision probability matrix for the system. The merged data is then passed to the 3D method of characteristics function CACTUS3D, which contains the FHR model. Most of the data manipulation is carried out by the HEAD module, which performs scattering cross-section temperature interpolation. However, when resonant isotopes are present, HEAD performs corrections based on the equivalence theorem relating a library of resonance integrals for each resonant absorber to the particular problem. This is accomplished through interpolating within a table of resonance integrals as a function of equivalent potential scattering cross-section and temperature. A more sophisticated model includes a scheme for representing resonance events through the subgroup treatment (known as PRES-RES in WIMS) that is devised around the resonance integral tabulation of the WIMS JEFF-3.1.2 library. Thus, most of the isotopes in the FHR benchmark are treated through the equivalence treatment, while resonant absorbers, such as uranium and hafnium are treated by the means of the subgroup method. However, not all isotopes of interest for this benchmark (molybdenum in particular) contain the needed information to perform such corrections due to their infrequent appearance in historical reactor physics models.

2.3. FHR benchmark comparisons

The multiplication factor results for Phase I-A cases for both GT and UCam can be found in Table 1. For the five out of six cases where both results are available, there is good agreement between these two participants, as well as among all participants. The exception is Case 3 which models the CR as being inserted. Cases 1 and 3 are identical aside from the absence or presence of the CR, respectively. However, while with no CR the difference between UCam to GT is only 202 ± 3 pcm, with the CR the magnitude of the difference is increased to 4040 ± 3 pcm.

GT Case 3 results agree well with those of other participants, some of which are using different codes and different cross section libraries. Specifically, two other participating institutions used Serpent with ENDF/B-VII.0 data and two used the 3D Monte Carlo code OpenMC [15] with ENDF/B-VII.1 data [16]. Not surprisingly, the other Serpent users had results which agreed well with the GT results with differences of 46 ± 18 and 78 ± 4 pcm for Case 3. Although consistent, this does not preclude the possibility that the issue is with the ENDF/B-VII.0 data since it was used by all participants modeling in Serpent. A comparison with the OpenMC results is more relevant since a separate code and nuclear data library were both used. The two OpenMC results had differences of 40 ± 9 and 58 ± 11 pcm with respect to the GT results, showing that all Monte Carlo results are consistent, while UCam results differed notably from the rest. Good agreement between GT and UCam results in all other cases (Case 3 being the exception) suggests the differences are due to the presence of the CR. Consistency of the geometric model was verified, thus leaving the CR cross sections used by WIMS as the main suspect. Additional simulations were conducted independent of the FHR benchmark and are presented and investigated further in the remainder of the paper.

3. Analysis of differences in spectra and reaction rates

Before performing further analyses looking into nuclear data and physics, it was important to confirm that both the GT and UCam models match. Since the cases with the CR withdrawn agree well, the model components beyond the CR region are likely not the source of error. Therefore, the focus shifted to the CR itself. A check confirmed that the dimensions as well as material compositions and densities used by the two benchmark participants matched. The difference however is that in GT's Serpent model, the seven naturally occurring isotopes of molybdenum are explicitly modeled with concentrations proportional to their respective natural abundances as specified in the FHR benchmark technical specifications, while in UCam's WIMS model elemental (natural molybdenum) cross sections are used. The elemental molybdenum data in the WIMS library is a predefined mixture of isotopic data from the JEFF-3.1.2 evaluation and is not related to the elemental data used in other evaluations (namely older ENDF/B distributions). The FHR benchmark comparison between the GT and UCam results showed that only Case 3 involving the use of a molybdenum-bearing MHC CR had significant differences despite otherwise good agreement for all other cases. Therefore, the rest of analysis considers only cases involving the CR inserted.

3.1. Additional simulations

So far, the molybdenum isotope cross section data included with ENDF/B-VII.0 has served as the reference data set. However, more recent releases in the ENDF/B lineage have included updated evaluations for two naturally occurring isotopes. With the release of ENDF/BVII.1 [16], new cross section data was introduced for ^{92}Mo and ^{95}Mo. It should be noted that no updates were made to naturally occurring molybdenum isotopes between the releases of

Table 1
Phase I-A multiplication factor results [6].

Case	k GT Serpent[a]	k UCam WIMS	Δk (UCam-GT) [pcm]	Average k[b]	σ(k)[b] [pcm]
Case 1	1.39559	1.39762	202	1.39454	237
Case 2H	1.40557	1.40650	93	1.40514	109
Case 2C	1.42065	1.42232	167	1.42066	126
Case 3	1.03205	0.99166	−4040	1.03084[c]	277[c]
Case 4	1.09886	[d]	[d]	1.09676	308
Case 4R	0.83969	[d]	[d]	0.83869	317
Case 5	0.80041	0.79975	−66	0.79911	319
Case 6	1.26301	[d]	[d]	1.26204	318
Case 7	1.50567	1.50828	261	1.50513	231

[a] All GT Serpent simulations had a reported statistical uncertainty of at most 3 pcm.
[b] These values were found by comparing the results of seven benchmark participants (six for cases where UCam WIMS results were either not available ([d]) or excluded ([c])). These columns serve to highlight the generally very good agreement among FHR benchmark participant results for all cases considered. Individual results from other participants aside from GT and UCam are not shown here but available elsewhere [6].
[c] UCam WIMS results are not included when calculating standard deviation for this case due to large observed differences.
[d] These cases were not simulated in WIMS due to modeling challenges with discrete burnable absorbing materials.

ENDF/B-VII.1 and ENDF/B-VIII.0. In order to isolate the impact of the molybdenum cross section changes between ENDF/B-VII.0 and ENDF/B-VII.1, a case was run using ENDF/B-VII.0 cross section data for all other materials used in the FHR assembly model except for the molybdenum data which was taken from ENDF/B-VII.1. This case is called "ENDF/B-VII.1 Mo Case 3".

Since the UCam WIMS results for benchmark Case 3 were generated using elemental molybdenum cross sections, the GT Serpent model switched to also using ENDF/B elemental molybdenum cross sections to draw closer to the usage of JEFF-3.1.2 elemental data by UCam in WIMS. Both use the sum-total of the seven individual molybdenum isotope atom densities (0.06368273 atom/(barn·cm)). This case is called "Elemental Case 3".

Elemental Case 3 provides a data point for the molybdenum concentrations used in the MHC CR. It was deemed useful to have an additional molybdenum-bearing case for supplementary comparison. To achieve this, the atom density of molybdenum was reduced from the reference elemental atom density to 0.03 atom/(barn·cm), representing about 53% reduction. This test case is referred to as "Reduced Mo".

To further preclude the possibility that anything other than molybdenum in the MHC CR is responsible for the differences between the GT and UCam results, it is important to run a test case devoid of molybdenum. This is accomplished by retaining the hafnium and carbon content of the CR and simulating a case with this material composition. While hafnium constitutes only 1.2% by weight of MCH, it has a significant thermal absorption cross section, and its impact on criticality is not negligible. This test case is referred to as "HC".

To confirm that the differences in the FHR benchmark CR test cases are driven by cross sections, it is necessary to rule out possible methodological issues with WIMS for the unusual FHR fuel assembly geometry. One possibility is that since the CR is optically thick, essentially a black absorber, the self-shielding method employed in the deterministic code WIMS might be challenged by the significant amount of self-shielding which occurs in the MHC. Another highly absorbing material, boron carbide (B_4C), was selected to be used in place of the MHC for a test case. If the B_4C results are problematic, that might point toward an issue with WIMS. If they are consistent, the observed FHR benchmark differences would almost certainly be driven by molybdenum cross sections. This case is referred to as "B_4C".

These additional test cases were independently simulated by GT and UCam to produce the results found in Table 2. The starting point is the first line, Benchmark Case 3 with its large discrepancy, previously presented in Table 1. The results of "ENDF/B-VII.1 Mo Case 3" show that the update to cross sections for ^{92}Mo and ^{95}Mo between ENDF/B-VII.0 and ENDF/B-VII.1 has an impact of 109 ± 4 pcm. This difference is relatively small compared to that observed for the UCam WIMS results, meaning discussions of results between WIMS and ENDF/B-VII.0 molybdenum cross sections can be extended to ENDF/B-VII.1 and ENDF/B-VIII.0 as well. Changing the GT Serpent model from using explicit isotopes to elemental molybdenum has a significant impact as shown in "Elemental Case 3". The change results in a reduction of the multiplication factor by 1378 ± 4 pcm, which is quite surprising since, if the cross sections used were generated from the same data sets, they should have yielded comparable results. Even with this large internal disparity between GT Serpent results, a still-larger difference of 2662 ± 3 pcm exists between the GT Serpent and UCam WIMS results. The "Reduced Mo" cases also have a large discrepancy of 1778 pcm. This difference is about 56% lower than that observed between the benchmark cases, which is approximately proportional to the density reduction, and supports the assumption that molybdenum cross sections are the main driver of the observed FHR benchmark differences. For the "HC" cases, there is good agreement between GT Serpent and UCam WIMS. With the molybdenum removed from the CR, a difference of 45 ± 4 pcm is quite acceptable. From the comparison of "B_4C" cases, it is evident that WIMS in fact accurately captures the self-shielding physics of the CR for other strong thermal neutron absorbing materials. Both the GT Serpent and UCam WIMS results are virtually identical with a difference of 9 ± 3 pcm. Based on these results, there is no question that the elemental molybdenum cross sections are responsible for the differences observed in the FHR benchmark. Further analysis of the MHC and HC test cases was conducted to investigate the physics behind the discrepancies.

3.2. Elemental molybdenum cross sections lineage

The case in Table 2 which stands out the most is "Elemental Case 3". Since the elemental cross sections are expected to be consistent with the natural abundance concentration of isotopic cross sections, the results should match those of a simulation using explicit isotopic natural abundance concentrations for the seven naturally occurring isotopes of molybdenum. However, as is evident from the GT Serpent cases for "Elemental Case 3" and "Benchmark Case 3", this is not what is observed. To answer why this was the case, the authors examined the data file for elemental molybdenum distributed with Serpent's ENDF/B-VII.0 [17] data. The file turns out to have been taken directly from ENDF/B-VI.8, because the official release of ENDF/B-VII.0 does not include an elemental molybdenum file. While it is common for data libraries to borrow the data file used in the preceding version for uncommonly used elements and isotopes, the borrowing process did not end there. The file was converted to ENDF-6 format in January 1990 for the release of ENDF/B-VI.0 in July 1990; untouched otherwise from the listing used in ENDF/B–V, which was made available in 1979. This ENDF/B–V version was based upon the ENDF/B-IV release of 1974 but only made updates to the capture cross section in the energy range from 1 keV to 20 MeV, leaving data below 1 keV unaltered. The final trace documentation in the data file states that the ENDF/B-IV data for energies below 1 keV were taken from ENDF/B-III, which was released in 1972.

As will become relevant to proceeding results and the discussion, there had been no updates to the ENDF elemental

Table 2
Multiplication factor for additional investigation cases.

Case	k_{eff}		Δk [pcm] (UCam − GT)
	GT Serpent	UCam WIMS	
Benchmark Case 3	1.03205 ± 0.00002	0.99165	−4040
ENDF/B-VII.1 Mo Case 3	1.03314 ± 0.00003	0.99165	−4149
Elemental Case 3	1.01827 ± 0.00003	0.99165	−2662
Reduced Mo	1.10148 ± 0.00003	1.08370	−1778
HC (No Mo)	1.22653 ± 0.00004	1.22608	−45
B_4C	1.00328 ± 0.00003	1.00319	−9

molybdenum cross section evaluation for neutron energies below 1 keV since, at best, 1972. A summary of when the seven naturally occurring molybdenum isotopes last had their cross section evaluations updated for commonly used data libraries can be found in Table 3. For feasibility reasons, evaluated libraries (including JEFF and ENDF/B) assess the quality of all available data prior to an official release and update them when possible. This explains why certain datasets within a lineage of evaluated libraries remains the same between releases if the data is still deemed acceptable given finite experimental resources. While the individual isotopes of molybdenum have had their respective cross section evaluations updated more recently, the elemental molybdenum cross section evaluation from the ENDF lineage is quite dated. As a note, as is the case with ENDF/B-VII.0, the official releases of ENDF/B-VII.1 and ENDF/B-VIII.0 both exclude a cross section data file for elemental molybdenum. Incident neutron cross section data files are only available for isotopes of molybdenum instead as elemental data has been phased out.

The elemental molybdenum cross sections used by WIMS are of particular interest because they are generated from the isotopic cross sections available in the JEFF 3.1.2 library. The official distribution of JEFF-3.1.2 does not include an elemental data file and cross sections are only provided for isotopes of molybdenum. The elemental molybdenum file included with JEFF-3.1.2 used by WIMS was created by the developers of WIMS using the individual isotope cross sections of JEFF-3.1.2 [14], which originally trace back to data from the release of JENDL-3.3. Thus, the WIMS elemental cross section file differs from the elemental cross section file found in the ENDF/B-VII.0 evaluation. However, many of the molybdenum isotope data files from JEFF-3.1.2 based on JENDL-3.3 borrow significantly from even earlier versions of JENDL libraries. Similar to the case with ENDF/B-VII.0, the elemental molybdenum cross section data used by WIMS likely contains values derived from a range of evaluations which could justify the differences observed. To clarify, this commentary is only applicable to the data for elemental molybdenum contained in the JEFF-3.1.2 library of WIMS and not to more recent libraries, which are continuously produced by ANSWERS as new evaluations are released. Since the likely culprit for the observed differences in the FHR benchmark has been identified as legacy cross sections, the rest of the paper will examine and quantitatively evaluate the impact of the dated cross sections.

3.3. Neutron spectrum in CR

The differences in neutron spectra for the CR inserted were examined to investigate the impact of the elemental molybdenum cross sections. The normalized GT Serpent and UCam WIMS neutron spectra over the entire FHR assembly geometry for Case 3 are depicted in Fig. 2. There is generally good agreement between the two codes, as spectral differences are quite small. The spectral results for Fig. 2 as well as those of Figs. 3–6 are scored using the XMAS LWPC 172 group structure [20]. This energy structure is supported by WIMS and is predefined for tallying within Serpent, which allows for direct comparisons between the two codes.

The fact that the spectral results have good agreement over the entire FHR geometry in Fig. 2 is not surprising due to the similarity seen between GT Serpent and UCam WIMS for other cases used in the FHR benchmark. A more insightful comparison is obtained by considering the neutron spectrum in only the CR region, as presented in Fig. 3 for both WIMS and Serpent results of the FHR Benchmark Case 3.

While the spectral profile should be informative to the reader for the general behavior of the flux, spectral differences allow for easier discernment between the two sets of results. In addition to the benchmark case shown in Fig. 3, the neutron spectrum was extracted from both WIMS and Serpent simulations for the Reduced Mo and HC cases as well. Spectral differences between the WIMS and Serpent results for the Benchmark, Reduced Mo, and HC cases are shown in Fig. 4. The authors have identified three regions of interest, all with energies below 1 keV, marked as 1, 2, and 3 in Fig. 4. The first region, within a single energy group, sees the largest magnitude of spectral difference (about 80%) between the Serpent and WIMS results. This narrow energy group has boundaries between 40.169 and 45.5174 eV. The second region of interest is a relatively broad energy group between 91.661 and 136.742 eV, which has a group difference of about 40% between the Serpent and WIMS results. The third region spans multiple energy groups with boundaries between 304.325 and 914.242 eV. In all three regions, the neutron flux reported by WIMS using elemental molybdenum cross sections is significantly depressed relative to the value reported by Serpent using explicit isotopic molybdenum cross sections. This suggests that the capture rate in the MHC CR is consequently higher to account for the depression, as will be investigated in the next section.

3.4. Capture reaction rate in CR

To confirm the source of spectral depressions observed in the WIMS results of Fig. 4, the (n,γ) neutron capture reaction rates were extracted from the UCam WIMS and GT Serpent results for the Benchmark, Reduced Mo, and HC cases. Differences between the WIMS and Serpent results for each case are shown in Fig. 5. As was done previously, the same three regions of interest are indicated in the figure. For the first and second regions which each correspond to a single energy group, large neutron capture reaction rate differences are observed as predicted. For the third region which spans multiple energy groups, all constituent groups appear to have a higher neutron capture rate reported by WIMS using elemental molybdenum cross sections than those of Serpent using explicit isotopic molybdenum cross sections. The HC results generally have much smaller differences than the cases with molybdenum. This supports the conclusion that the differences are only due to the elemental molybdenum cross sections and not the other materials present in the MHC CR. The neutron capture reaction rates are driven by the neutron capture macroscopic cross section, which is further examined in the next section.

Table 3
Evaluation dates for isotopes of molybdenum from commonly-used data libraries.

	JEFF-3.1.2 [13]	JEFF-3.2 [18]	JEFF-3.3 [18]	ENDF/B-VII.0 [12]	ENDF/B-VII.1 [16]	ENDF/B-VIII.0 [19]
^{92}Mo	Aug. 1989	Aug. 1989	Mar. 2009	Aug. 1989	May 2011	May 2011
^{94}Mo	Aug. 1989	Aug. 1989	Mar. 2009	Feb. 2005	Feb. 2005	Feb. 2005
^{95}Mo	Oct. 2003	Oct. 2003	Dec. 2010	Feb. 2006	Dec. 2010	Dec. 2010
^{96}Mo	Aug. 1989	Aug. 1989	Mar. 2009	Aug. 1989	Aug. 1989	Aug. 1989
^{97}Mo	Feb. 2005	Feb. 2005	Mar. 2009	Feb. 2005	Feb. 2005	Feb. 2005
^{98}Mo	Aug. 1989	Aug. 1989	Mar. 2009	Aug. 1989	Aug. 1989	Aug. 1989
^{100}Mo	Aug. 1989	Aug. 1989	Mar. 2009	Aug. 2000	Aug. 2000	Aug. 2000

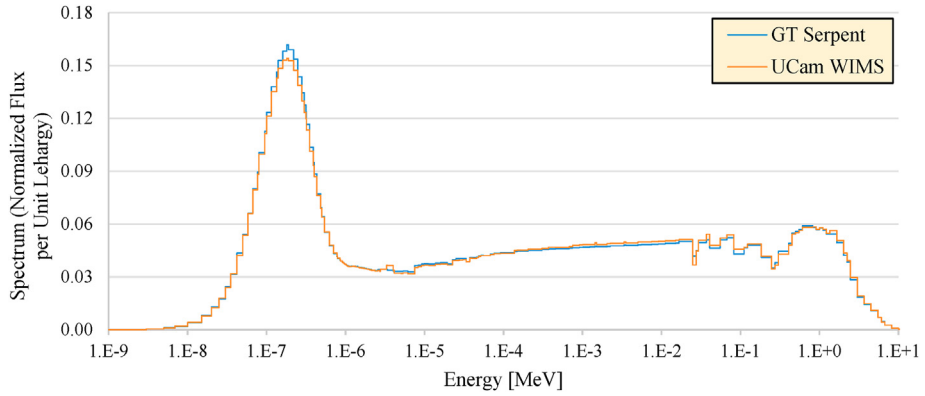

Fig. 2. Normalized flux per unit lethargy in the entire assembly for FHR Benchmark Case 3 in WIMS and Serpent.

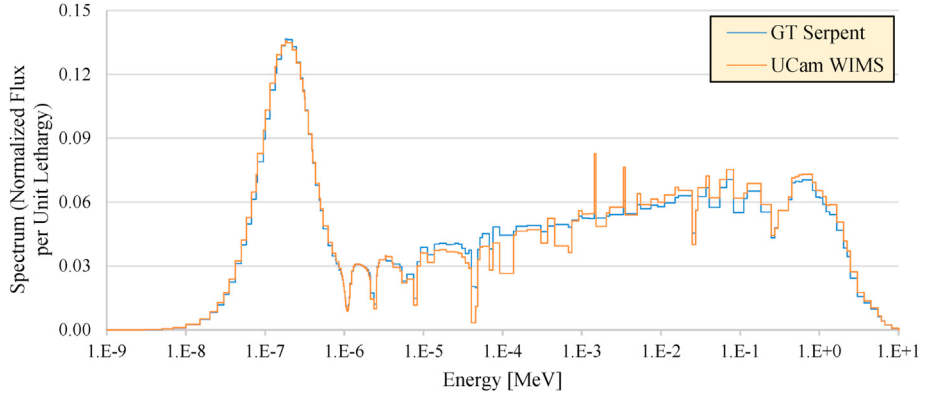

Fig. 3. Normalized flux per unit lethargy in the CR for FHR benchmark Case 3 in WIMS and Serpent.

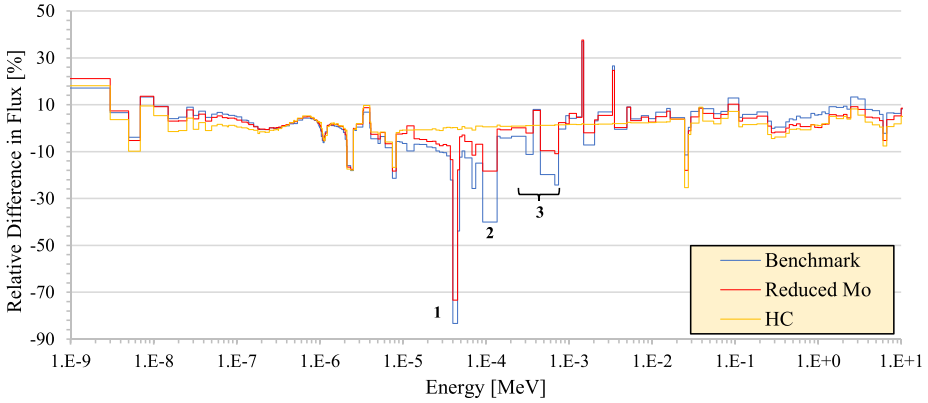

Fig. 4. Difference in normalized neutron flux in CR of UCam WIMS relative to GT Serpent.

3.5. CR capture cross section

The neutron capture macroscopic cross sections (Σ_γ) were obtained from the UCam WIMS and GT Serpent results for the Benchmark, Reduced Mo, and HC cases. The ratio between the WIMS and Serpent results for each case are shown in Fig. 6. Once again, the same three regions of interest are indicated in Fig. 6. For the first region, the Σ_γ used by WIMS in the Benchmark case is about 9.95 times larger than that used by Serpent; differing by almost an order of magnitude. For the second region, the Σ_γ used by WIMS in the Benchmark case is about 6.8 times larger than that used by Serpent. In the third region which spans several energy groups, the WIMS Σ_γ results are consistently at least double the value of their Serpent counterparts.

The significant differences in Σ_γ between WIMS using elemental molybdenum and Serpent using explicit isotopic molybdenum cross sections can likely be traced back to the processing of large resonances of individual molybdenum isotopes. Fig. 7 shows the microscopic neutron capture cross sections (σ_γ) for the seven naturally occurring isotopes of molybdenum extracted from ENDF/

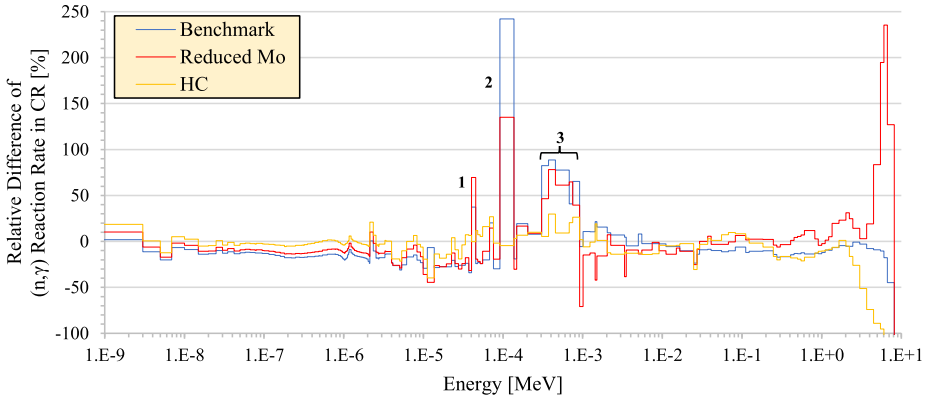

Fig. 5. Difference in (n,γ) reaction rate in CR of UCam WIMS relative to GT Serpent.

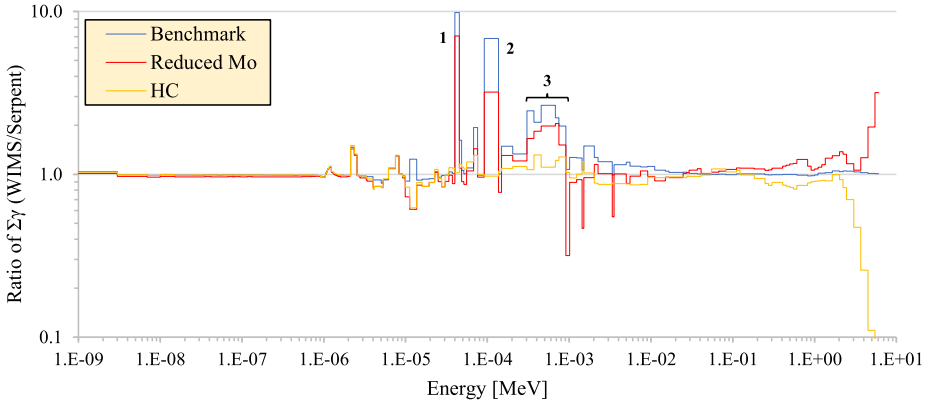

Fig. 6. Ratio of Σ_γ in CR for UCam WIMS relative to GT Serpent.

B-VII.0 [21]. Each of the three regions of interest from the prior figures aligns with strong resonance behavior of σ_γ. The first region corresponds with a relatively large resonance in ^{95}Mo. The second region corresponds with a large resonance in ^{97}Mo. The third region corresponds with several resolved resonances in six of the naturally occurring molybdenum isotopes (all but ^{94}Mo). The large differences observed in the FHR benchmark results can be traced back to strong resonances in isotopes of molybdenum.

4. Conclusion

In recent years, there has been significant interest in molten salt technology. Next generation reactor designs such as MSRs and FHRs require modeling and simulation tools capable of accurately

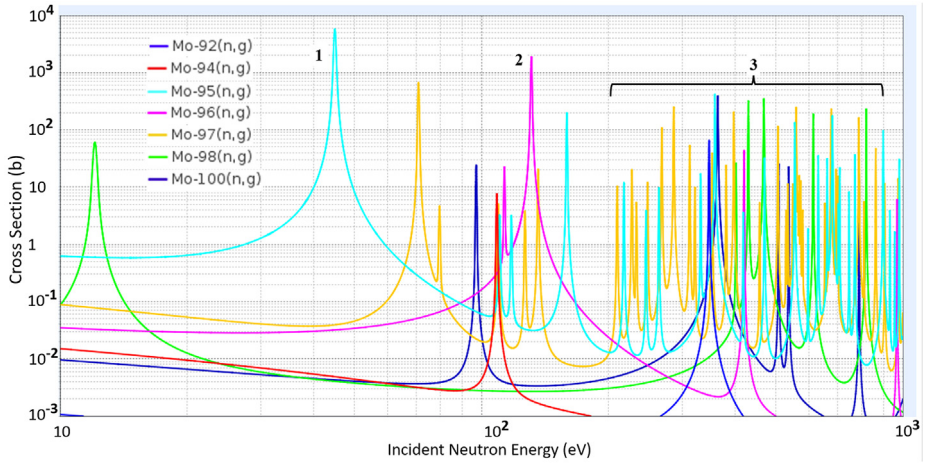

Fig. 7. Microscopic neutron capture cross sections for isotopes of molybdenum [21].

capturing core physics phenomena to study these systems, which is not a trivial task due to their geometric complexity and novel materials. This need prompted the creation of the FHR benchmark, under the auspices of OECD-NEA, to evaluate the readiness of existing methods and codes for analyzing FHR-like reactor designs. Several participating members contributed results to the initial phase of the FHR benchmarking process with generally good agreement considering that each participant blindly modeled the FHR system using the simulation tool of their choice.

The exception to the good agreement was Case 3 which modeled an MHC CR as inserted. Significant differences in the multiplication factor were observed in both WIMS and Serpent between using elemental molybdenum cross sections for a molybdenum-bearing CR and using explicit isotopic cross sections with natural molybdenum isotopic abundances. Investigation into the ENDF/B-VII.0 data used by Serpent revealed that the elemental cross section evaluation was quite dated, with certain energy regions being updated only as recently as 1972 with the release of ENDF/B-III. More recent nuclear data library releases (e.g., ENDF/B-VII.1, ENDF/B-VIII.0, and others) have phased-out legacy elemental molybdenum cross sections by excluding them altogether. This is consistent with cross sections for other nuclides that are now typically provided only for individual isotopes. Users should be aware if using elemental molybdenum cross sections, that even though they were formally included in some ENDF/B-VII.0-based libraries, they are likely actually based on rather dated legacy elemental molybdenum cross sections, which may result in significant inaccuracies. Clearly, the impact will be more pronounced in systems containing significant amount of molybdenum, whether in control elements, or in advanced fuel designs.

Additional simulations were performed to supplement the cases used in the FHR benchmark. Through use of a different CR material B_4C, excellent agreement between WIMS and Serpent was obtained suggesting that both could accurately capture the strong self-shielding effect in the CR. Leaving the elemental molybdenum cross sections as the only culprit for large observed differences, studies considered the impact on neutron spectrum, neutron capture reaction rate, and macroscopic neutron capture cross section all within the CR. For the FHR spectrum, elemental molybdenum cross sections underpredict the capture rate for low energies (0.01–90 eV except for a single energy group near a strong resonance of ^{95}Mo between 40 and 45 eV) and significantly overpredict the capture rate for resonance energies including the aforementioned 40–45 eV group, 90–135 eV, and the energy range from 300 to 900 eV which spans multiple considered energy groups. Future work could focus on either obtaining or recreating identical cross section data libraries for use in WIMS and Serpent, which could provide additional insights into the observed modeling differences.

When modeling molybdenum in an FHR-like system, and in general in systems containing non-trivial amount of molybdenum, care should be taken to check the molybdenum cross section provenance and actual evaluation date since some libraries offer fairly dated elemental cross sections. Moreover, that fact is not necessarily obvious from the cross section data file name. Molybdenum isotopic cross sections are generally more recent, and presumably more accurate. More recently released data libraries (e.g., ENDF/B-VII.1 and ENDF/B-VIII.0) do not include elemental molybdenum cross sections whatsoever with their distribution, thus eliminating the possibility of using old elemental data. However, the default data library for WIMS JEFF-3.1.2 only has the option to use elemental molybdenum cross section data, which has shown to be problematic through the analyses of this paper. It is expected that the treatment of the molybdenum similar to that of the other resonant isotopes (i.e., resonance treatment by means of equivalence theory or subgroup method) would provide better performance. Stemming from the results of this work and serving as a resolution to the identified issues, the developers of the WIMS code package have extended the initially available JEFF-3.1.2 library to contain the isotopic data used to create the elemental molybdenum data. This extended library is not included in standard distributions of WIMS libraries because there has not been, prior to this work, a documented physics benefit on results, while it involves additional computational cost. Users of WIMS should be aware of its existence in particular if it has potential to be relevant to their own work; we are planning to test and employ it within the future FHR benchmark efforts.

Declaration of competing interest

The authors declare that they have no known competing financial interests or personal relationships that could have appeared to influence the work reported in this paper.

Acknowledgements

The presented work is part of a broader effort to benchmark FHR modeling and simulations involving seven team members from four countries [5,6]. The benchmark is performed under the auspices of OECD NEA; the support of Mr. Ian Hill (Deputy Head, Division of Nuclear Science) is gratefully acknowledged.

References

[1] P.N. Haubenreich, J.R. Engel, Experience with the molten-salt reactor experiment, Nucl. Appl. Technol. 8 (2) (1970) 118–136.
[2] D.T. Ingersoll, C.W. Forsberg, L.J. Ott, D.F. Williams, J.P. Renier, D. Wilson, S.J. Ball, L. Reid, W.R. Corwin, G.D. Del Cul, P.F. Peterson, H. Zhao, P.S. Pickard, E.J. Parma, M. Vernon, Status of Preconceptual Design of the Advanced High-Temperature Reactor (AHTR), Oak Ridge National Laboratory, Oak Ridge, Tennessee, 2004. Report ORNL/TM-2004/104.
[3] D.E. Holcomb, D. Ilas, V.K. Varma, A.T. Cisneros, R.P. Kelly, J.C. Gehin, Core and Refueling Design Studies for the Advanced High Temperature Reactor, Oak Ridge National Laboratory, Oak Ridge, Tennessee, 2011. Report ORNL/TM-2011/365.
[4] V.K. Varma, D.E. Holcomb, F.J. Peretz, E.C. Bradley, D. Ilas, A.L. Qualls, N.M. Zaharia, AHTR Mechanical, Structural, and Neutronic Preconceptual Design, Oak Ridge National Laboratory, Oak Ridge, Tennessee, 2012. Report ORNL/TM-2012/320.
[5] B. Petrovic, K. Ramey, I. Hill, Benchmark Specifications for the Fluoride-Salt High-Temperature Reactor (FHR) Reactor Physics Calculations: Phase 1-A and I-B: Fuel Element 2D Benchmark, vol. 5, Nuclear Science, OECD Publishing, Paris, France, 2020. NEA/NSC/R, 2021.
[6] B. Petrovic, K. Ramey, I. Hill, E. Losa, M. Elsawi, Z. Wu, C. Lu, J. Gonzales, D. Novog, G. Chee, K. Huff, M. Margulis, N. Read, E. Shwageraus, Preliminary results of the NEA FHR benchmark phase I-A and I-B (fuel element 2D benchmark), in: The International Conference on Mathematics and Computational Methods Applied to Nuclear Science and Engineering, Raleigh, NC, 2021.
[7] J. Leppänen, et al., The Serpent Monte Carlo code: status, development and applications in 2013, Ann. Nucl. Energy 82 (2015) 142–150.
[8] B.A. Lindley, J.G. Hosking, D.J. Powney, B.S. Tollit, T.D. Newton, R. Perry, T.C. Ware, P.N. Smith, Current status of the reactor physics code WIMS and recent developments, Ann. Nucl. Energy 102 (2017) 148–157.
[9] F. Rahnema, B. Petrovic, P. Singh, P. Burke, H. Noorani, X. Sun, G. Yoder, P. Tsvetkov, J. Zhang, D. Zhang, D. Ilas, "The Challenges in Modeling and Simulation of Fluoride Salt Cooled High Temperature Reactors," White Paper CRMP-2017-9-001, Georgia Institute of Technology, Atlanta, GA, USA, 2017.
[10] K.M. Ramey, B. Petrovic, Monte Carlo modeling and simulations of AHTR fuel assembly to support V&V of FHR core physics methods, Ann. Nucl. Energy 118 (2018) 272–282.
[11] B. Petrovic, T. Flaspoehler, K. Ramey, Benchmarking FHR core physics simulations: 2D fuel assembly model, in: Proc. 12th Intl. Conf. On Nuclear Option in Countries with Small and Medium Electricity Grids, June 3-6, Zadar, Croatia, 2018.
[12] M.B. Chadwick, P. Oblozinsky, M. Herman, N.M. Greene, R.D. McKnight, D.L. Smith, P.G. Young, R.E. MacFarlane, G.M. Hale, S.C. Frankle, A.C. Kahler, T. Kawano, R.C. Little, D.G. Madland, P. Moller, R.D. Mosteller, P.R. Page, ENDF/B-VII.0: next generation evaluated nuclear data library for nuclear science and technology, Nucl. Data Sheets 107 (12) (2006) 2931–3060.
[13] O. Cabellos, Processing and validation of JEFF-3.1.2 cross-section library into various formats: ACE, PENDF, GENDF, MATXSR and BOXER, Nucl. Data Sheets

118 (2014) 456–458.
[14] The ANSWERS Software Service, WIMS A Modular Scheme for Neutronics Calculations - User Guide for Version 10, ANSWERS/WIMS/REPORT/014, 2015.
[15] P.K. Romano, N.E. Horelik, B.R. Herman, A.G. Nelson, B. Forget, K. Smith, OpenMC: a state-of-the-art Monte Carlo code for research and development, Ann. Nucl. Energy 82 (2015) 90–97.
[16] M.B. Chadwick, M. Herman, P. Oblozinsky, M.E. Dunn, Y. Danon, A.C. Kahler, D.L. Smith, B. Pritychenko, G. Arbanas, R. Arcilla, R. Brewer, D.A. Brown, R. Capote, A.D. Carlson, Y.S. Cho, H. Derrien, K. Guber, G.M. Hale, P. Young, ENDF/B-VII.1 nuclear data for science and technology: cross sections, covariances, fission product yields and decay data, Nucl. Data Sheets 112 (12) (2011) 2887–2996.
[17] R.J. Howerton, F. Schmittroth, R.E. Schenter, Material 4200 Incident Neutron Data, National Nuclear Data Center, Jan 1990 [Online]. Available: https://www-nds.iaea.org/public/download-endf/ENDF-B-VI-8/NEUTRON/mat/endf-b-vi-8_n_4200.txt. (Accessed 13 February 2021). Accessed.
[18] A.J.M. Plompen, O. Cabellos, C. De Saint Jean, The joint evaluated fission and fusion nuclear data library, JEFF-3.3, The European Physical Journal A 56 (2020).
[19] D.A. Brown, M.B. Chadwick, R. Capote, A.C. Kahler, A. Trkov, M.W. Herman, A.A. Sonzogni, Y. Danon, A.D. Carlson, M. Dunn, D.L. Smith, G.M. Hale, G. Arbanas, R. Arcilla, C.R. Bates, B. Beck, B. Becker, F. Brown, Y. Zhu, ENDF/B-VIII.0: the 8th major release of the nuclear reaction data library with CIELO-project cross sections, new standards and thermal scattering data, Nucl. Data Sheets 148 (2018) 1–142.
[20] XMAS LWPC 172-group structure [Online]. Available: http://serpent.vtt.fi/mediawiki/index.php/XMAS_LWPC_172-group_structure. (Accessed 7 February 2021). Accessed.
[21] Table of Nuclides, Nuclear data center at KAERI [Online]. Available, http://atom.kaeri.re.kr/nuchart/#. (Accessed 7 February 2021).